RSC Advances

PAPER

View Article Online
View Journal | View Issue

Cite this: *RSC Adv.*, 2017, **7**, 30725

Hydrothermal conversion of high-concentrated glycerol to lactic acid catalyzed by bimetallic $CuAu_x$ ($x = 0.01–0.04$) nanoparticles and their reaction kinetics†

Lingqin Shen, Xin Zhou, Aili Wang, * Hengbo Yin, * Haixu Yin and Wanjing Cui

Catalytic hydrothermal conversion of highly concentrated glycerol to lactic acid was investigated over bimetallic $CuAu_x$ ($x = 0.01–0.04$) nanoparticle catalysts. The bimetallic $CuAu_x$ nanoparticles were prepared by the wetness chemical reduction method and characterized by XRD, TEM, HRTEM, XPS, and atomic absorption spectrophotometry techniques. Metallic Cu and Au nanoparticles coalesced to form secondary bimetallic nanoparticles with an alloy trend. The bimetallic $CuAu_x$ nanoparticles exhibited higher catalytic activity for the conversion of highly concentrated glycerol (2–3 mol L^{-1}) to lactic acid than both sole monometallic Cu and Au nanoparticles, probably due to the alloying tendency between the metallic Cu and Au nanoparticles. When the reaction was carried out with the initial glycerol and NaOH concentrations of 3.0 and 3.3 mol L^{-1} at 200 °C for 2 h, the yields of lactic acid over the bimetallic $CuAu_2$, $CuAu_3$, and $CuAu_4$ catalysts were above 83% and the formation rate of lactic acid was more than 0.17 mol g_{cat}^{-1} h^{-1}. The carbon balance values ranged from 89.2% to 92.9%. The reaction activation energies for glycerol conversion over the bimetallic $CuAu_1$, $CuAu_2$, $CuAu_3$, and $CuAu_4$ catalysts were 64.0, 53.4, 46.8, and 36.9 kJ mol^{-1}, respectively. The hydrothermal conversion of high-concentrated glycerol to lactic acid catalyzed by the bimetallic $CuAu_x$ nanoparticles is an alternative to the conventional fermentation process starting from carbohydrate.

Received 19th April 2017
Accepted 7th June 2017

DOI: 10.1039/c7ra04415a

rsc.li/rsc-advances

1. Introduction

To replace the traditional fossil energy sources by sustainable energy, biodiesel, the first-generation biofuel, is being produced on a large scale worldwide. However, glycerol as a by-product, is largely produced in the biodiesel production *via* the transesterification of vegetable oil or animal fat with methanol. In the transesterification process, the production capacity of glycerol is *ca.* 10–20% of raw material in weight.[1–3] Currently, in the United States, the biodiesel industry produces *ca.* 7.6 billion liters of glycerol each year,[1,4] which is oversupplied in the market. Although the second-generation biofuels obtained from ligno-cellulose biomass and the third-generation biofuels produced from algae-derived biomass have been paid a great attention in Europe,[5] production of the first-generation biofuels still steadily increases with the production amount of 9.9 billion liters in Europe because their production is cheaper than those of the second and third generation biofuels.[6,7] Glycerol production is produced in quantities of more than 1 billion liters per year in Europe. Effective conversion of the oversupplied biomass glycerol to high valued chemicals has attracted great attention of researchers.[8]

Many valuable glycerol derivatives, such as lactic acid, 1,3-propanediol, 1,2-propanediol, and succinic acid, can be synthesized through various catalytic processes.[1,2] Notably, selective dehydrogenation of glycerol to lactic acid is an attractive research topic because lactic acid has been widely used in food, pharmaceutical, leather, cosmetic, textile, and biodegradable polymer (polylactic acid) fields.[2] Polylactic acid has the potential to replace conventional petroleum-based polyethylene terephthalate plastics due to its biocompatibility and biodegradability.[8] It is estimated that the market demand of polylactic acid will be *ca.* 150 000 tons by 2017 and 400 000 tons by 2022.[9]

Nowadays, lactic acid is mainly produced by the fermentation technique using sugar as feedstock at a concentration of 10 wt%.[10] Although the fermentation process gives a high lactic acid yield of 90%, it is facing challenges in relatively high level of the production cost, low efficiency, waste disposal issues, and worldwide food shortage. As an alternative to the conventional fermentation process, catalytic conversion of glycerol to lactic acid becomes a hot research topic.

The catalytic conversion of glycerol to lactic acid can be categorized into homogeneous and heterogeneous catalysis

Faculty of Chemistry and Chemical Engineering, Jiangsu University, Zhenjiang 212013, China. E-mail: yin@ujs.edu.cn; alwang@ujs.edu.cn; Tel: +86-0-511-88787591

† Electronic supplementary information (ESI) available. See DOI: 10.1039/c7ra04415a

methods. For the homogeneous catalysis method, it was reported that when the hydrothermal conversion of glycerol (0.33 mol L^{-1}) was catalyzed by NaOH in an aqueous solution at 300 °C, the lactic acid yield of 90% was obtained.[11] It was found that alkali metal hydroxides exhibited higher catalytic activity than alkaline earth metal hydroxides. Ramírez-López *et al.*[12] reported that the lactic acid yield of 84.5% was obtained when the hydrothermal conversion of glycerol (2.5 mol L^{-1}) was carried at 280 °C for 1.5 h with a NaOH/glycerol mole ratio of 1.1 : 1. According to the above-mentioned results, NaOH as a homogeneous catalyst exhibited good catalytic activity for the hydrothermal conversion of glycerol to lactic acid. However, high reaction temperature was the drawback for the homogeneous conversion of glycerol to lactic acid.

Heterogeneously catalytic conversion of glycerol to lactic acid has been investigated over various supported noble and non-noble metal catalysts. When Pt/ZrO_2 was used as the catalyst for conversion of glycerol to lactic acid at 180 °C in a NaOH aqueous solution under anaerobic condition, the highest yield of lactic acid was 84%.[13] When $AuPt/TiO_2$, Au/CeO_2, and $PtAu/CeO_2$ were used as the catalysts to catalyze aerobic oxidation of glycerol at 90 °C in a NaOH aqueous solution, the maximum yields of lactic acid of 27%, 81%, and 79% were obtained, respectively.[14–16] The synergistic effect between Au and Pt improved catalytic activity in glycerol oxidation to lactic acid. It was reasonable to conclude that noble metal catalysts exhibited high catalytic activities for the conversion of glycerol to lactic acid at a lower reaction temperature under aerobic or anaerobic condition. However, considering the high cost and scarcity of noble metals, exploring an efficient catalyst with a lower cost is highly necessary.

Recently, the conversion of glycerol to lactic acid over Cu-based catalysts[17–19] with a lower cost and a high catalytic activity was investigated. When the hydrothermal conversion of glycerol (1.1 mol L^{-1}) in a NaOH aqueous solution was carried out at 240 °C for 6 h, the lactic acid selectivities of 79.7%, 78.6%, and 78.1% at the glycerol conversions of 75.2%, 97.8%, and 93.6% were obtained using Cu/SiO_2, CuO/Al_2O_3, and Cu_2O as catalysts, respectively.[17] In our previous work, Cu/hydroxyapatite and Cu nanoparticles were used as the catalysts for hydrothermal conversion of glycerol to lactic acid at 230 °C with the initial glycerol concentration of 1 mol L^{-1}, the lactic acid selectivities reached 90% and 92% at the glycerol conversions of 91% and 98%, respectively.[18,19] However, in the viewpoint of economy, the low glycerol concentration may lead to a risk in industrial application.

In our present work, bimetallic $CuAu_x$ nanoparticles were prepared by the wetness chemical reduction method and characterized by XRD, TEM, HRTEM, XPS, and atomic absorption spectrophotometer techniques. In the bimetallic $CuAu_x$ nanoparticles, the Cu and Au nanoparticles coalesced to form secondary bimetallic nanoparticles with alloy trend. The bimetallic $CuAu_x$ nanoparticles effectively catalyzed the conversion of high-concentrated glycerol to lactic acid at a relative low reaction temperature in a batch reactor. The reaction kinetics for glycerol conversion over the $CuAu_x$ nanoparticles were also analyzed.

2. Experimental

2.1. Materials

The chemicals, anhydrous ethanol, sodium hydroxide, copper nitrate trihydrate ($Cu(NO_3)_2 \cdot 3H_2O$), hexadecyl trimethyl ammonium bromide (CTAB), chloroauric acid ($HAuCl_4 \cdot 3H_2O$) hydrazine hydrate ($N_2H_4 \cdot H_2O$, 85%), glycerol, lactic acid, 1,2-propanediol, formic acid, acetic acid, oxalic acid, and isopropyl alcohol were of reagent grade and were purchased from Sinopharm Chemical Reagent Co., Ltd. All the chemicals were used as received without further purification. Deionized water was used through all the experiments.

2.2. Preparation of catalysts

Bimetallic $CuAu_x$ nanoparticle catalysts (x mole of Au to 100 mole of Cu) were prepared by the wetness chemical reduction method. One gram of $CuAu_x$ nanoparticle catalyst was prepared by reducing copper nitrate trihydrate and chloroauric acid with hydrazine hydrate in anhydrous ethanol. A given amount of copper nitrate and organic modifier (CTAB) (the weight ratio of CTAB to copper nitrate, 1 : 10) were dissolved in 30 mL of anhydrous ethanol by ultrasonic treatment for 30 min. In a thermostatic bath, the solution was preheated to 55 °C under stirring. An ethanol solution of NaOH (1.0 M, 20 mL) was added dropwise to adjust the pH value of the reaction solution to 8–9. After that, an ethanol solution of hydrazine hydrate (8 mL in 80 mL anhydrous ethanol) was added dropwise to the reaction solution under mild stirring for 2.5 h. After the reaction mixture was cooled down to 30 °C, 20 mL of chloroauric acid aqueous solution with given concentration was added dropwise to the reaction mixture under mild stirring for 0.5 h. After reaction, the reaction mixture was cooled down to room temperature. The as-prepared bimetallic $CuAu_x$ nanoparticles were filtrated and washed with anhydrous ethanol for three times to remove the organic modifier and kept in an anhydrous ethanol solution before they were characterized and used as the catalysts for hydrothermal conversion of glycerol to lactic acid. The as-prepared bimetallic $CuAu_x$ nanoparticles were donated as $CuAu_1$, $CuAu_2$, $CuAu_3$, and $CuAu_4$, respectively. x was the mole number of metallic Au to 100 mol of metallic Cu in the bimetallic $CuAu_x$ nanoparticles.

Monometallic Cu and Au nanoparticles were also prepared according to the above-mentioned method, correspondingly. The properties of the monometallic Cu, monometallic Au, and bimetallic $CuAu_x$ nanoparticle catalysts are listed in Table 1.

2.3. Characterization of catalyst

The powder X-ray diffraction (XRD) patterns of the monometallic Cu, monometallic Au, and bimetallic $CuAu_x$ samples were recorded on a diffractometer (D8 super speed Bruke-AEX Company, Germany) using Cu Kα radiation (λ = 1.54056 Å) with Ni filter, scanning from 10° to 85° (2θ). The crystallite sizes of Cu^0 (1 1 1) and Au^0 (1 1 1) in the bimetallic $CuAu_x$ nanoparticle catalysts were calculated according to the Scherrer's equation, $D = K\lambda/(B \cos \theta)$. The value of K was taken 1.0 and B was the full width of the diffraction line at half of the maximum

Table 1 Physicochemical properties of nanoparticle catalysts

Catalysts	Cu/Au atomic ratios[a]	Cu/Au atomic ratios from XPS	Particle sizes of Cu and Au[b] (nm)		Crystallite sizes of Cu and Au[c] (nm)		Binding energies (eV)			
			Cu	Au	Cu (1 1 1)	Au (1 1 1)	Cu2p$_{1/2}$	Cu2p$_{3/2}$	Au4f$_{5/2}$	Au4f$_{7/2}$
Cu			13.2	—	17.8		952.4	932.6		
$CuAu_1$	100 : 0.99	100 : 1.55	13.0	4.0	17.5	4.5	952.3	932.5	87.5	83.8
Spent$CuAu_1$	100 : 0.99				17.6	4.6				
$CuAu_2$	100 : 1.98	100 : 2.46	13.0	4.0	15.6	4.8	952.1	932.3	87.4	83.9
Spent $CuAu_2$	100 : 1.93				15.6	4.9				
$CuAu_3$	100 : 2.98	100 : 5.12	13.0	5.0	17.2	5.4	952.0	932.1	87.6	83.9
Spent $CuAu_3$	100 : 2.87				17.3	5.4				
$CuAu_4$	100 : 3.96	100 : 9.59	12.0	6.0	16.9	6.3	951.7	931.8	87.6	83.9
Spent$CuAu_4$	100 : 3.95				17.1	6.4				
Au				6.2					87.7	84.0

[a] Cu/Au atomic ratios were analyzed by atomic absorption spectrophotometer. [b] The particle sizes of Cu and Au were determined by TEM and HRTEM. [c] The crystallite sizes of Cu and Au were calculated by Scherrer's equation.

of XRD peak of metallic Cu^0 (1 1 1) or Au^0 (1 1 1). The crystallite sizes are listed in Table 1.

The X-ray photoelectron spectra (XPS) of the monometallic Cu, monometallic Au, and bimetallic $CuAu_x$ samples were recorded on an ESCALAB 250 spectrometer (PHI5000VersaProbe, UlVAC-PHI Company, Japan) using Al Kα radiation at 1486.6 eV. The binding energies of Cu and Au of the samples were calculated with respect to C1s peak at 284.6 eV.

The transmission electron microscopy (TEM) and high-resolution transmission electron microscopy (HRTEM) images were obtained on a microscope (JEM-2100) operated at an acceleration voltage of 200 kV to investigate the microstructures and the crystal structures of the monometallic Cu, monometallic Au, and bimetallic $CuAu_x$ samples. To prepare TEM specimens, the sample was dispersed in an anhydrous ethanol *via* ultrasonic equipment for 10 min, then a drop of the ethanol suspension was placed onto a copper grid coated with a layer of amorphous carbon. The particle sizes of the Cu and Au nanoparticles were measured from the TEM and HRTEM images by counting at least 150 individual particles. The average particle sizes of the Cu and Au nanoparticles were calculated by a weighted-average method according to the individual particle sizes of all the counted particles.[19,20]

The atomic ratios of Cu/Au of the fresh and spent bimetallic $CuAu_x$ samples were analyzed on an atomic absorption spectrophotometer (TAS-986). The results are listed in Table 1.

2.4. Catalytic test

To investigate the catalytic activities of the monometallic Cu, monometallic Au, and bimetallic $CuAu_x$ nanoparticles, a 100 mL of aqueous solution of glycerol and NaOH and an appointed amount of nanoparticle sample were charged into a 300 mL stainless steel autoclave with a mechanical stirrer. And the autoclave was flushed with N_2 to replace air inside for 10 min. The stirring speed was set at 600 rpm. The reaction time was counted without temperature rising time period and the reaction mixture was heated to the desired temperature in *ca.* 0.5 h. After reacting for an appointed time period, the reaction mixture was cooled down to room temperature with cooling water through a coil in the reactor.

The reaction mixture was filtered before analyzing the concentrations of reactant and products. The filtrate was acidified with hydrochloric acid (37%) to the pH value of 2–3 and diluted with deionized water for HPLC analysis. A gas-phase chromatograph (SP-6800A) equipped with a PEG-20 M packed capillary column (0.25 mm × 30 m) and a FID was used to analyze the concentrations of the unreacted glycerol and produced 1,2-propanediol using isopropyl alcohol as the internal standard. The products, lactic acid, acetic acid, oxalic acid, and formic acid, were analyzed on an Agilent HPLC system equipped with a tunable absorbance UV detector and a reverse-phase column (Innoval ASB C18, 5 μm, 100 Å, 4.6 × 250 mm) at 30 °C. The mobile phase was a methanol aqueous solution (10 : 90, v/v) with a flow rate of 0.8 mL min^{-1}. The pH value of the mobile phase was 2.3, which was adjusted with phosphate buffer. The detection wavelength was set at 210 nm. The

product selectivity was calculated by carbon balance. The catalytic test for each catalyst was repeated for at least twice in order to ensure the accuracy of the data. The following equation was used to calculate the product selectivity.

$$\text{Product selectivity} = \frac{(\text{mole of product})(\text{carbon number of product molecule})}{3(\text{mole of consumed glycerol})} \quad (1)$$

3. Results and discussion

3.1. XRD analysis

The XRD patterns of the monometallic Cu, monometallic Au, and fresh and spent bimetallic $CuAu_x$ samples with different Au contents prepared by the wet chemical reduction method are shown in Fig. 1. The XRD peaks of the monometallic Cu sample appearing at $2\theta = 43.3$, 50.4, and 74.1° were indexed as the (1 1 1), (2 0 0), and (2 2 0) planes of face centered-cubic (fcc) copper (JCPDS 04-0836), respectively. The XRD peaks of the metallic Au sample appearing at $2\theta = 38.2$, 44.3 64.7, and 77.6° were indexed as the (1 1 1), (2 0 0), (2 2 0), and (3 1 1) planes of face centered-cubic (fcc) gold (JCPDS 46-1043). The XRD peaks of Cu present in the fresh bimetallic $CuAu_1$, $CuAu_2$, $CuAu_3$, and $CuAu_4$ samples appeared at $2\theta = 43.5$–43.4, 50.7–50.4, and 74.4–74.1°, respectively. And no diffraction peaks of copper oxides or copper hydroxides were detected, indicating that metallic Cu nanoparticles were formed in the metallic $CuAu_x$ nanoparticles. The XRD peaks of Cu present in the fresh $CuAu_x$ catalysts slightly shifted to low values with the increase in Au contents. It is reasonable to conclude that there was an interaction between Cu and Au nanoparticles. The XRD peaks of Au present in the fresh bimetallic $CuAu_1$, $CuAu_2$, $CuAu_3$, and $CuAu_4$ samples appeared at $2\theta = 38.4$, 44.5 (shoulder), 64.9, and 77.8°, which were higher than those of the monometallic Au sample by 0.2°. As compared to the XRD peaks of monometallic Au sample, the XRD peak shifts of Au in the bimetallic $CuAu_x$ nanoparticle catalysts indicated that there probably existed an alloy trend between Cu and Au. The alloy trend between Cu and Au means that there was an interaction between Cu nanoparticle and Au nanoparticle. TEM analysis also shows that Au nanoparticles anchored at the surfaces of Cu nanoparticles, which was discussed in the following section.

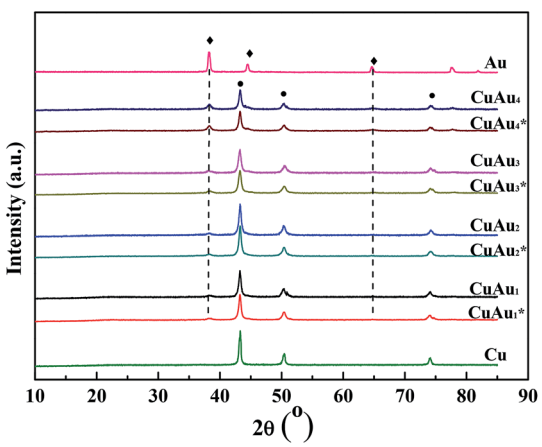

Fig. 1 XRD patterns of the monometallic Cu, monometallic Au, and fresh and spent bimetallic CuAu catalysts. ●, Cu^0; ◆, Au^0; *, spent catalysts.

The crystallite sizes of the monometallic Cu, monometallic Au, and fresh bimetallic $CuAu_x$ nanoparticle samples were estimated by the Scherrer's equation (Table 1). The crystallite sizes of Cu (1 1 1) and Au (1 1 1) of these samples were around 17 and 5 nm, respectively. The results revealed that small-sized metallic Cu and Au nanoparticles were formed in our present samples.

After taking part in the reaction, the XRD patterns of the spent $CuAu_x$ nanoparticle catalysts and the crystallite sizes of Cu (1 1 1) and Au (1 1 1) calculated by the Scherrer's equation were close to those of the fresh ones, indicating that the chemical structures of the $CuAu_x$ nanoparticle catalysts did not change under our present reaction conditions.

3.2. XPS analysis

To determine the chemical states of $CuAu_x$ nanoparticles, the XPS measurement was employed. The XPS of Cu2p and Au4f regions are shown in Fig. 2 and the binding energies are listed in Table 1.

For the bimetallic $CuAu_1$, $CuAu_2$, $CuAu_3$ and $CuAu_4$ samples, the binding energies of $Cu2p_{1/2}$ and $Cu2p_{3/2}$ were 952.3, 932.5 eV; 952.1, 932.3 eV; 952.0, 932.1 eV; and 951.7, 931.8 eV, respectively, which were lower than those (952.4 eV for $Cu2p_{1/2}$, 932.6 eV for $Cu2p_{3/2}$) of monometallic Cu sample. The binding energies of $Cu2p_{1/2}$ and $Cu2p_{3/2}$ of the bimetallic $CuAu_x$ samples decreased with increasing the Au content (Fig. 2a). The binding energies of $Au4f_{5/2}$ and $Au4f_{7/2}$ of the monometallic Au sample were 87.7 and 84.0 eV, respectively. The binding energies of $Au4f_{5/2}$ and $Au4f_{7/2}$ of the bimetallic $CuAu_1$, $CuAu_2$, $CuAu_3$, and $CuAu_4$ samples were 87.5, 83.8; 87.4, 83.9; 87.6, 83.9; and 87.6, 83.9 eV, respectively (Fig. 2b). The Au4f binding energies of the bimetallic $CuAu_x$ samples were decreased by 0.1 eV as compared to those of the monometallic Au sample. As compared to the monometallic Cu and Au nanoparticles, the binding energy shifts of Cu2p and Au4f of the bimetallic $CuAu_x$ nanoparticles were probably due to the alloy trend between Cu and Au nanoparticles, which was consistent with the conclusion obtained by XRD analysis. The Cu/Au atomic ratios of the $CuAu_x$ samples obtained by XPS analysis were obviously lower than those obtained by atomic absorption spectrophotometer, respectively, indicating that the Au nanoparticles coated on the surfaces of Cu nanoparticles (Table 1).

The binding energy values of metallic Cu and Cu^+ are almost the same as each other, the metallic Cu and Cu^+ species cannot be distinguished directly according to their binding energy values. To ascertain the chemical states of the copper species present in the monometallic Cu and bimetallic $CuAu_x$ nanoparticles, the Wagner plots are drawn and shown in Fig. 2c. The kinetic energy (KE) of the Auger transition and the $Cu2p_{3/2}$ binding energy of the photoemission were on Y and X axes,

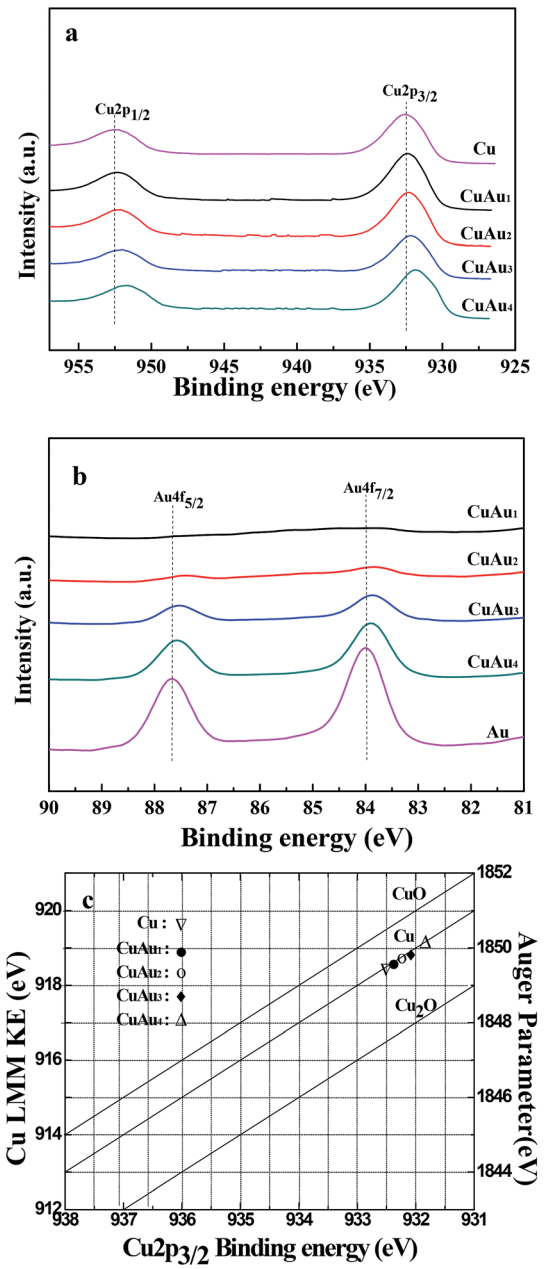

Fig. 2 XPS spectra of (a) Cu2p, (b) Au4f, and (c) Wagner plots of the monometallic Cu, monometallic Au, and bimetallic CuAu nanoparticles.

respectively. The data for Cu, Cu_2O, and CuO reference samples were taken from the ref. 21 and 22. According to Fig. 2c, the Auger parameters of the monometallic Cu and bimetallic $CuAu_x$ nanoparticles fell on the line of metallic copper, which indicated that the copper species in the nanoparticles were in metallic state, being consistent with the conclusion obtained by XRD analysis.

3.3. TEM and HRTEM analyses

The TEM and HRTEM images (or SAED pattern) of the monometallic Cu, monometallic Au, and bimetallic $CuAu_x$ nanoparticles are shown in Fig. 3. Fig. 3a1 and a2 show the TEM image and SAED pattern of the monometallic Cu nanoparticles. The TEM image shows that the Cu nanoparticles were spherical with the average particle size of 13.2 nm and the particle size distribution of 3–48 nm (Table 1). According to the SAED analysis (Fig. 3a2), the diffraction fringes were examined to be close to the {1 1 1} (0.209 nm), {2 0 0} (0.181 nm), {2 2 0} (0.128 nm), and {3 1 1} (0.111 nm) lattice spacings of fcc copper, respectively. The as-prepared monometallic Cu nanoparticles had a polycrystalline structure.

The TEM and HRTEM images of the monometallic Au sample shows that the spherical Au nanoparticles were formed with the average particle size of 6.2 nm and the particle sizes ranging from 3 to 10 nm (Fig. 3f1 and f2). The lattice fringes of the Au nanoparticles were examined to be 0.203 (0.204) and 0.236 (0.237) nm, being close to the {2 0 0}and {1 1 1} lattice spacings of fcc metallic gold.

Fig. 3b1–e1 and b2–e2 show the TEM and HRTEM images of the bimetallic $CuAu_x$ samples. It was observed that the irregular particulates were constructed by the coalescence of Cu and Au nanoparticles. The average particle sizes of Cu and Au nanoparticles in the bimetallic $CuAu_x$ samples were around 13 and 5 nm, respectively.

For the bimetallic $CuAu_1$ sample, the lattice fringes of 0.180 and 0.208 (0.210) nm were detected, which were close to the {2 0 0} and {1 1 1} lattice spacings of fcc metallic copper. The lattice fringes of 0.204 and 0.231 (0.235) nm were close to the {2 0 0} and {1 1 1} lattice spacings of fcc metallic gold.

The lattice fringes of 0.180 (0.183) and 0.210 nm for the bimetallic $CuAu_2$ sample were close to the {2 0 0} and {1 1 1} lattice spacings of fcc metallic copper while the lattice fringes of 0.202 and 0.238 (0.239) nm were close to the {2 0 0} and {1 1 1} lattice spacings of fcc metallic gold.

For the $CuAu_3$ sample, the lattice fringes of 0.182 and 0.207 nm were close to the {2 0 0} and {1 1 1} lattice spacings of fcc metallic copper while the lattice fringes of 0.142, 0.198, and 0.233 nm were close to the{2 2 0}, {2 0 0}, and {1 1 1} lattice spacings of fcc metallic gold.

For the $CuAu_4$ sample, the lattice fringes of 0.180 (0.181) and 0.210 nm were corresponding to the {2 0 0} and {1 1 1} lattice spacings of fcc metallic copper while the lattice fringes of 0.201 (0.204) and 0.233 nm were corresponding to the {2 0 0} and {1 1 1} lattice spacings of fcc metallic gold.

The TEM and HRTEM images show that both metallic Cu and Au nanoparticles were formed in the bimetallic $CuAu_x$ nanoparticles. The bimetallic $CuAu_x$ nanoparticles were formed by the coalescence of Cu and Au nanoparticles, indicating that there was probably an interaction between Cu and Au nanoparticles.

3.4. Hydrothermal conversion of glycerol to lactic acid

3.4.1. Catalytic activities of monometallic Cu, monometallic Au, and bimetallic $CuAu_x$ nanoparticles. To investigate the effect of Cu/Au ratios in the bimetallic $CuAu_x$ nanoparticles on the catalytic conversion of glycerol to lactic acid, the catalytic reaction over the nanoparticles was carried out in 100 mL of glycerol (2 mol L^{-1}) aqueous solution with the NaOH/glycerol

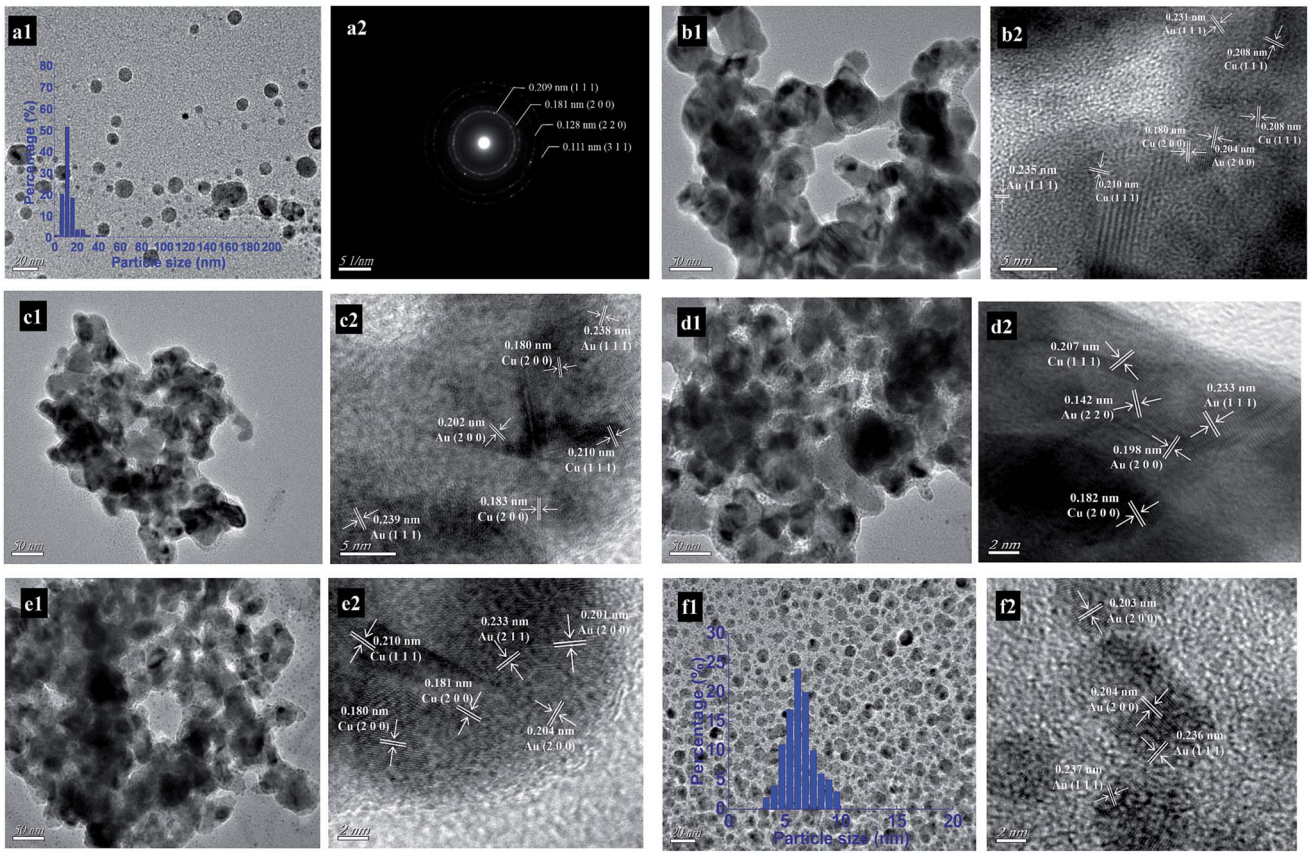

Fig. 3 TEM and HRTEM images of (b1–e1, b2–e2) bimetallic CuAu nanoparticles, TEM and SAED images of (a1 and a2) monometallic Cu, and TEM and HRTEM images of (f1 and f2) monometallic Au.

mole ratio of 1.1 : 1 and 0.736 g of catalyst at 200 °C for 2 h. The experimental results are listed in Table 2. Lactic acid was formed as the main product and small amount of oxalic acid, formic acid, acetic acid, and 1,2-propanediol as by-products was detected. H_2 was formed in gas phase.

When NaOH and the bimetallic $CuAu_x$ catalyst were added in the reaction solution together, the conversions of glycerol were more than 97% with the lactic acid selectivities of above 87% (Table 2). However, when sole NaOH or sole bimetallic $CuAu_2$ catalyst was added in the reaction solution, only trace amount of glycerol was converted (Table S1†). It was reasonable to conclude that NaOH and bimetallic $CuAu_x$ catalyst synergistically catalyzed the conversion of glycerol to lactic acid. The synergistic effect of NaOH and metallic catalyst on the glycerol conversion to lactic acid was also observed when metallic Cu was used as the catalyst in a NaOH aqueous solution.[18,19]

Table 2 The effect of Cu/Au ratios on catalytic conversion of glycerol

Catalysts	Conversions[a] (%)	Selectivities (%)					Activities for glycerol consumption[b] (mol mol_{cat}^{-1} h^{-1})	Activities for lactic acid formation[c] (mol mol_{cat}^{-1} h^{-1})	Carbon balances[d] (%)	Residual carbon[e] (wt%)
		Lactic acid	Oxalic acid	Formic acid	Acetic acid	1,2-Propanediol				
Cu	67.2	80.3	0.3	1.1	0.8	1.5	5.8	4.7	84.0	
$CuAu_1$	97.2	89.3	0.5	0.8	0.7	0.2	8.6	7.7	91.5	2.4
$CuAu_2$	99.0	93.8	0.3	0.6	0.4	0.3	9.0	8.4	95.4	0.3
$CuAu_3$	99.3	90.3	0.5	1.0	0.9	0.4	9.2	8.3	93.1	3.2
$CuAu_4$	100	87.2	0.7	1.3	1.1	0.6	9.4	8.2	90.9	0.4
Au[f]	18.3	66.4	1.0	1.7	1.2	0.8	9.8	6.5	71.1	

[a] Reaction conditions: glycerol aqueous solution, 2.0 mol L^{-1}, 100 mL; NaOH/glycerol molar ratio 1.1 : 1; catalyst, 0.736 g; reaction temperature 200 °C; reaction time, 2.0 h. The catalyst compositions are listed in Table 1. [b] Glycerol conversion activities normalized per metal atom. [c] Lactic acid formation activities normalized per metal atom. [d] Carbon balances were calculated according to both detected products and reacted glycerol. [e] Residual carbon was analyzed by the FLASH1112A element analyzer. [f] The amount of monometallic Au catalyst was equal to the amount of Au in the $CuAu_4$ catalyst.

When the monometallic Cu nanoparticles and monometallic Au nanoparticles (the amount of Au equal to that in the $CuAu_4$ catalyst) were used as catalysts, the conversions of glycerol and selectivities of lactic acid were 67.2%, 80.3%; 18.3%, 66.4%, respectively. The conversions of glycerol and selectivities of lactic acid over the bimetallic $CuAu_x$ catalysts were higher than those over the monometallic Cu and Au nanoparticles.

The catalytic activities of the bimetallic $CuAu_x$ catalysts for glycerol conversion were 1.48–1.62 times that of the monometallic Cu nanoparticle catalyst (Table 2). The catalytic activities of the bimetallic $CuAu_x$ catalysts for glycerol conversion increased with the increase in Au contents. And the catalytic activity of the $CuAu_4$ catalyst for glycerol conversion was comparable to that of the monometallic Au catalyst with the same Au loading.

The catalytic activities of the bimetallic $CuAu_x$ catalysts for lactic acid formation were 1.63–1.79 times that of the monometallic Cu nanoparticle catalyst and were 1.18–1.29 times that of the monometallic Au nanoparticle catalyst, respectively (Table 2). The bimetallic $CuAu_x$ catalysts exhibited higher catalytic activity for the conversion of glycerol to lactic acid than both monometallic Cu and Au nanoparticle catalysts. It is reasonable to suggest that the interaction between Cu and Au nanoparticles in the bimetallic $CuAu_x$ catalysts played an important role for the conversion of glycerol to lactic acid.

The carbon balance values over the bimetallic $CuAu_x$ catalysts were above 90% while over the monometallic Cu and Au catalysts, the values were 84% and 71.1%, respectively. The results revealed that the bimetallic $CuAu_x$ catalysts favored the formation of the useful chemicals and decreased the formation of polymer-like chemicals and the decomposition of resultant products. The residual carbon on the bimetallic $CuAu_x$ catalysts was less than 3.3%, indicating that only a small amount of polymer-like chemicals was deposited on the catalyst surfaces.

3.4.2. Effect of reaction time. The conversions of glycerol and selectivities of products with the reaction time are shown in Fig. 4 and S1.† When the bimetallic $CuAu_1$, $CuAu_2$, $CuAu_3$, and $CuAu_4$ nanoparticles were used as the catalysts, with prolonging the reaction time periods from 1 to 4 h, the conversions of glycerol increased from 60.2% to 100%, 76.4% to 100%, 80.1% to 100%, and 88.2% to 100%, respectively (Fig. 4a). The maximum lactic acid selectivities of 91.3%, 94%, 92.8%, and 89.4% were obtained after reacting for 1 h, respectively (Fig. 4b). With prolonging the reaction time to 4 h, the selectivities of lactic acid decreased to 80.9%, 82.9%, 79.3%, and 76.2%. The selectivities of oxalic, formic, acetic acid, and 1,2-propanediol over he bimetallic $CuAu_x$ catalysts were less than 1.6%, respectively (Fig. S1a–d†). The carbon balances over these bimetallic $CuAu_x$ catalysts decreased from *ca.* 94% to 84% upon prolonging the reaction time from 1 to 4 h (Fig. 4c). Over the bimetallic $CuAu_2$ catalysts, high carbon balances in a range of 85.6–95.7% were obtained. Prolonging the reaction time period probably caused the decomposition of resultant products to carbonate.

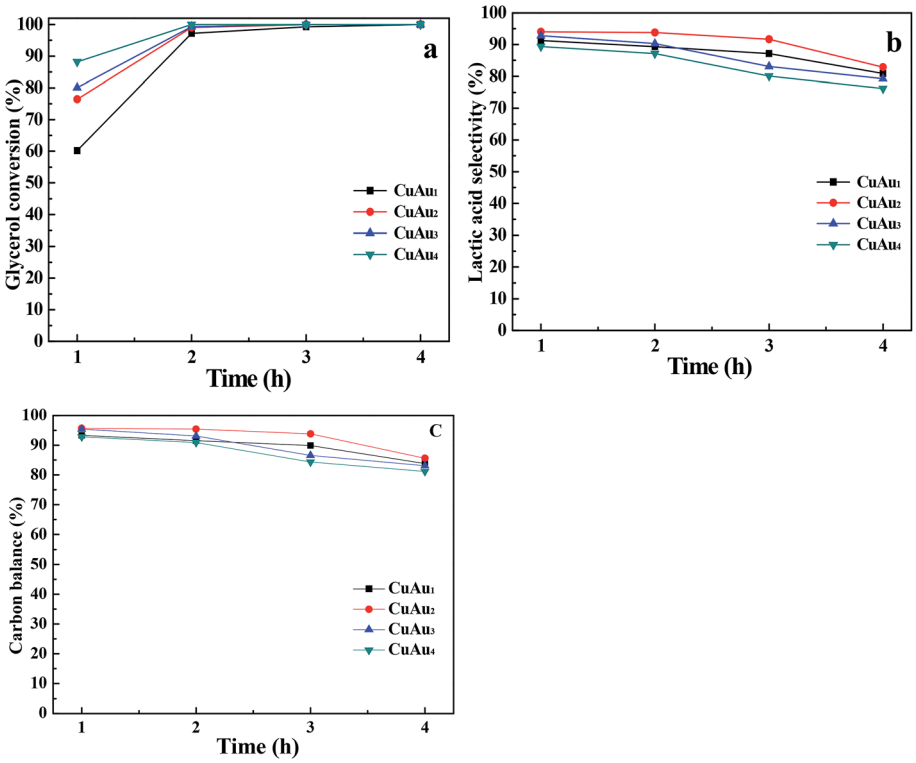

Fig. 4 Catalytic conversion of glycerol catalyzed by the bimetallic $CuAu_x$ nanoparticle catalysts. Reaction conditions: 100 mL of glycerol aqueous solution with the glycerol concentration of 2 mol L^{-1}, NaOH/glycerol mole ratio of 1.1 : 1, 0.736 g of catalyst, and reaction temperature at 200 °C. (a) Glycerol conversion; (b) lactic acid selectivity; (c) carbon balance.

Considering that after reacting for 2 h, high yield of lactic acid was obtained over the bimetallic $CuAu_x$ catalysts, the reaction time period was fixed at 2 h to investigate the effect of other reaction parameters on the catalytic conversion of glycerol to lactic acid.

3.4.3. Effect of reaction temperature. The results for the hydrothermal conversion of glycerol to lactic acid catalyzed by the bimetallic $CuAu_x$ nanoparticles at different reaction temperatures for 2 h are shown in Fig. 5 and S2.† The conversions of glycerol over the $CuAu_1$, $CuAu_2$, $CuAu_3$, and $CuAu_4$ catalysts increased from 67.5% to 99.3%, 88.8% to 100%, 90% to 100%, and 92.8% to 100%, respectively (Fig. 5a), with increasing the reaction temperature from 160 to 220 °C. The selectivities of lactic acid increased from 70.9% to 89.3%, 79.9% to 93.8%, 82.7% to 90.3%, and 83.4% to 87.2% with increasing the reaction temperatures from 160 to 200 °C, respectively (Fig. 5b). With further increasing the reaction temperature to 220 °C, the selectivities of lactic acid decreased to 86.4%, 86.9%, 82.1%, and 80.7%. The selectivities of by-products, such as oxalic acid, formic acid, acetic acid, and 1,2-propanediol, were less than 1.6%, respectively (Fig. S2†). Although high reaction temperature favored the catalytic conversion of glycerol, the reaction temperature at 200 °C may be favorable from the perspective of lactic acid yield. Furthermore, the carbon balances over the bimetallic $CuAu_x$ catalysts exhibited maximum values of *ca.* 93% at 200 °C (Fig. 5c). It could be explained as that at a lower reaction temperature, polymer-like chemicals and/or intermediate products were probably formed while at a higher reaction temperature, resultant products probably decomposed to carbonate.

3.4.4. Effect of glycerol concentration. The hydrothermal conversions of glycerol and selectivities of products over the bimetallic $CuAu_x$ catalysts under different glycerol concentrations are listed in Table 3. With increasing the glycerol concentrations to 3.0 mol L^{-1}, the conversions of glycerol over $CuAu_1$, $CuAu_2$, $CuAu_3$, and $CuAu_4$ catalysts decreased to 90.1%, 95.8%, 96.0%, and 97.4%, respectively. The selectivities of lactic acid decreased to 80.7%, 90.9%, 88.4%, and 85.7%. The selectivities of oxalic acid, formic acid, acetic acid, and 1,2-propanediol were less than 1.4%, respectively. At a low glycerol concentration, more catalytic active sites available on the surfaces of the bimetallic $CuAu_x$ catalysts led to effective conversion of glycerol to lactic acid. However, at a high glycerol concentration of 3.0 mol L^{-1}, the yields of lactic acid over the bimetallic $CuAu_2$, $CuAu_3$, and $CuAu_4$ catalysts were above 83% and the formation rate of lactic acid was more than 0.17 mol g_{cat}^{-1} h^{-1}. The carbon balance values ranged from 89.2% to 92.9%. The results revealed that the bimetallic $CuAu_x$ catalysts effectively catalyzed the conversion of high concentrated glycerol to lactic acid with a high formation rate of lactic acid.

The catalytic activities for glycerol conversion over the bimetallic $CuAu_x$ catalysts increased upon increasing the glycerol concentration. The bimetallic $CuAu_2$, $CuAu_3$, and $CuAu_4$ catalysts exhibited similar catalytic activities. However, these

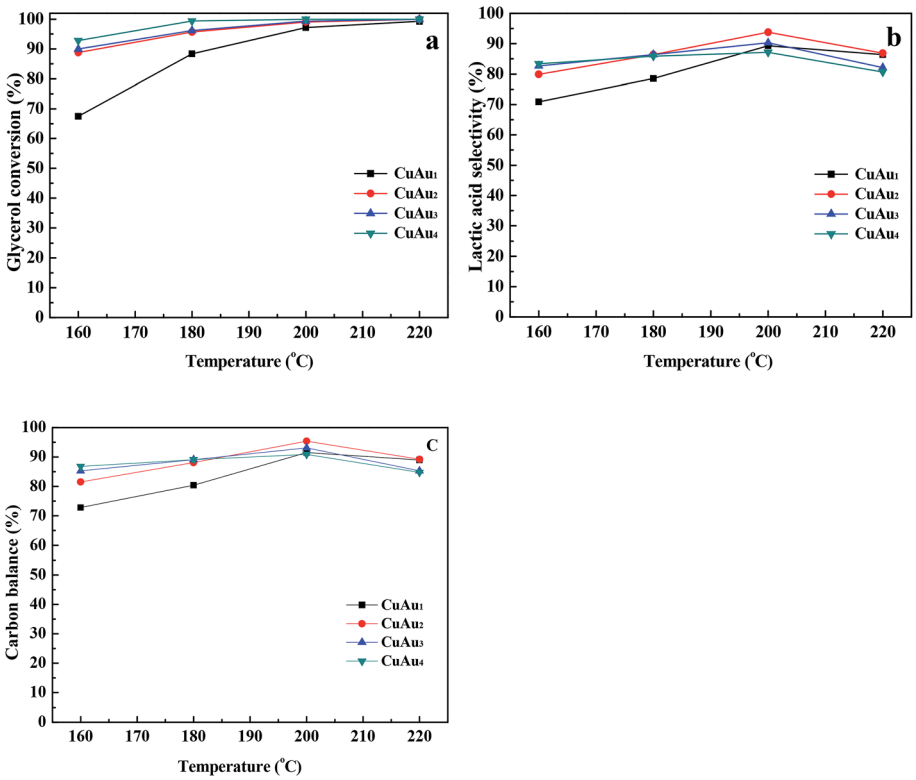

Fig. 5 Catalytic conversion of glycerol catalyzed by the bimetallic $CuAu_x$ nanoparticle catalysts. Reaction conditions: 100 mL of glycerol aqueous solution with the glycerol concentration of 2 mol L^{-1}, NaOH/glycerol mole ratio of 1.1 : 1, 0.736 g of catalyst, and reaction time of 2 h. (a) Glycerol conversion; (b) lactic acid selectivity; (c) carbon balance.

Table 3 Effect of glycerol concentration on catalytic conversion of glycerol[a]

Catalysts	Glycerol concentrations (mol L^{-1})	Glycerol conversions (%)	Selectivities (%)					Activities for glycerol consumption[b] (mol mol_{cat}^{-1} h^{-1})	Carbon balances[c] (%)
			Lactic acid	Oxalic acid	Formic acid	Acetic acid	1,2-Propanediol		
$CuAu_1$	1.5	99.2	91.8	0.7	0.9	0.9	0.2	6.6	94.5
	2.0	97.2	89.3	0.5	0.8	0.7	0.2	8.6	91.5
	2.5	94.7	86.9	0.3	0.6	0.7	0.4	10.5	88.9
	3.0	90.1	80.7	0.3	0.6	0.4	1.0	12.0	83.0
$CuAu_2$	1.5	100	94.0	0.5	0.7	0.6	0.3	6.8	96.1
	2.0	99.0	93.8	0.3	0.6	0.4	0.3	9.0	95.4
	2.5	97.5	92.3	0.3	0.5	0.4	0.6	11.0	94.1
	3.0	95.8	90.9	0.2	0.4	0.3	1.1	13.0	92.9
$CuAu_3$	1.5	100	92.5	0.8	1.2	1.3	0.3	6.9	96.1
	2.0	99.3	90.3	0.5	1.0	0.9	0.4	9.2	93.1
	2.5	98.7	89.0	0.4	0.7	0.7	0.7	11.4	91.5
	3.0	96.0	88.4	0.3	0.7	0.6	1.0	13.3	91.0
$CuAu_4$	1.5	100	91.9	1.0	1.4	1.4	0.4	7.0	96.1
	2.0	100	87.2	0.7	1.3	1.1	0.6	9.4	90.9
	2.5	99.3	87.0	0.6	1.0	1.1	0.9	11.6	90.6
	3.0	97.4	85.7	0.5	0.8	0.9	1.3	13.7	89.2

[a] Reaction conditions: glycerol aqueous solution, 100 mL; NaOH/glycerol mole ratio,1.1 : 1; catalyst loading, 0.736 g; reaction temperature, 200 °C; reaction time, 2.0 h. [b] Glycerol conversion activities normalized per metal atom. [c] Carbon balances were calculated according to both detected products and reacted glycerol.

catalysts exhibited higher catalytic activities than the $CuAu_1$ catalyst. An appropriate Au content was necessary for improving the catalytic activity of bimetallic $CuAu_x$ catalyst.

3.4.5. Effect of NaOH/glycerol mole ratio. When the hydrothermal conversion of glycerol was catalyzed by the bimetallic $CuAu_1$, $CuAu_2$, $CuAu_3$, and $CuAu_4$ catalysts with

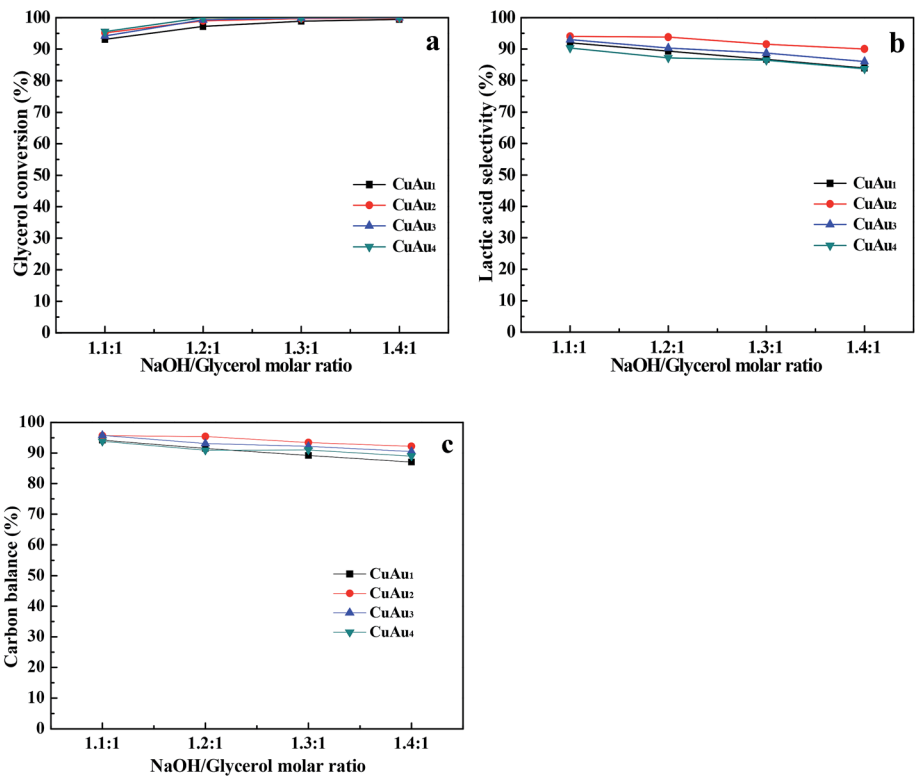

Fig. 6 Catalytic conversion of glycerol catalyzed by the bimetallic $CuAu_x$ nanoparticle catalysts. Reaction conditions: 100 mL of glycerol aqueous solution with the glycerol concentration of 2 mol L^{-1}, 0.736 g of catalyst, reaction temperature at 200 °C, and reaction time of 2 h. (a) Glycerol conversion; (b) lactic acid selectivity; (c) carbon balance.

different NaOH/glycerol mole ratios at 200 °C for 2 h, with increasing the NaOH/glycerol mole ratios from 1.1 : 1 to 1.4 : 1, the glycerol conversions increased from 93.1% to 99.5%, 95.2% to 99.8%, 94.2% to 100%, and 95.6% to 100%, respectively (Fig. 6a). And the selectivities of lactic acid decreased from 92.0% to 83.9%, 94.0% to 90.0%, 93.0% to 86%, and 90.3% to 83.7%, respectively (Fig. 6b). The selectivities of all the measured by-products were less than 1.9% (Fig. S3†). The carbon balances over these catalysts decreased from *ca.* 95% to 90% upon increasing NaOH/glycerol mole ratio from 1.1 : 1 to 1.4 : 1 (Fig. 6c). High NaOH concentration probably caused the decomposition of resultant products to carbonate.[12] The results revealed that high NaOH/glycerol mole ratio favored the hydrothermal conversion of glycerol. But excessive NaOH decreased the selectivity of lactic acid.

3.4.6. Effect of catalyst loading. The conversions of glycerol and selectivities of products in the catalytic conversion of glycerol to lactic acid over the bimetallic $CuAu_x$ catalysts with the loadings of 0.368–0.920 g at 200 °C for 2 h are listed in Table 4. For the bimetallic $CuAu_1$ catalyst, the conversions of glycerol and the selectivities of lactic acid increased from 87.8% to 99.6% and from 75.6% to 90.6%, respectively, with increasing the catalyst loadings from 0.368 g to 0.920 g. When the bimetallic $CuAu_2$, $CuAu_3$, and $CuAu_4$ nanoparticles were used as catalysts, glycerol was completely converted at the catalyst loadings of 0.92, 0.92, and 0.736 g, respectively. The maximum

Table 4 Effect of catalyst loading on catalytic conversion of glycerol[a]

Catalysts	Catalyst loadings (g)	Glycerol conversions (%)	Selectivities (%)					Activities for glycerol consumption[b] (mol mol_{cat}^{-1} h^{-1})	Carbon balances[c] (%)
			Lactic acid	Oxalic acid	Formic acid	Acetic acid	1,2-Propanediol		
$CuAu_1$	0.368	87.8	75.6	0.3	0.4	0.2	0.5	15.6	77.0
	0.552	91.5	86.3	0.5	0.7	0.4	0.5	10.8	88.4
	0.736	97.2	89.3	0.5	0.8	0.7	0.2	8.6	91.5
	0.920	99.6	90.6	0.7	1.0	0.8	0.2	7.1	93.3
$CuAu_2$	0.368	90.5	84.2	0.1	0.4	0.3	0.7	16.4	85.7
	0.552	95.5	92.9	0.3	0.5	0.4	0.3	11.5	94.4
	0.736	99.0	93.8	0.3	0.6	0.4	0.3	9.0	95.4
	0.920	100.0	83.6	0.5	0.8	0.7	0.2	7.2	85.8
$CuAu_3$	0.368	93.2	88.5	0.3	0.7	0.4	0.9	17.2	90.8
	0.552	97.4	91.4	0.5	0.9	0.6	0.6	12.0	94.0
	0.736	99.3	90.3	0.5	1.0	0.9	0.4	9.2	93.1
	0.920	100.0	79.6	0.8	1.3	1.0	0.3	7.4	83.0
$CuAu_4$	0.368	93.9	90.0	0.5	0.9	0.6	1.2	17.6	93.2
	0.552	98.6	87.9	0.6	1.1	0.7	0.7	12.3	91.0
	0.736	100.0	87.2	0.7	1.3	1.1	0.6	9.4	90.9
	0.920	100.0	77.4	1.2	1.6	1.4	0.5	7.5	82.1

[a] Reaction conditions: glycerol aqueous solution, 2.0 mol L^{-1}, 100 mL; NaOH/glycerol mole ratio, 1.1 : 1; reaction temperature, 200 °C; reaction time, 2.0 h. [b] Glycerol conversion activities normalized per metal atom. [c] Carbon balances were calculated according to both detected products and reacted glycerol.

Table 5 Hydrothermal conversion of glycerol to lactic acid over various catalysts

Catalysts	Initial concentrations ($mol \cdot L^{-1}$)		Reaction temperatures (°C)	Reaction time (h)	Glycerol conversions (%)	Lactic acid yields (%)	Ref.
	glycerol	NaOH					
—	0.33	1.25	300	1.5	—	90	11
—	2.5	2.75	280	2.5	~98	84.5	12
Pt/ZrO_2	0.54	1.0	180	24	94.0	84	13
Au/TiO_2	0.22	0.88	90	—	~30	22.1	14
Pt/TiO_2	0.22	0.88	90	—	~30	25.4	14
$AuPt/TiO_2$	0.22	0.88	90	—	~30	25.7	14
$AuPt/CeO_2$	0.17	0.68	100	0.5	99.0	79.2	16
Cu/SiO_2	1.1	1.21	240	6	75.2	59.9	17
Cu/HAP	1.0	1.1	230	2	91.0	81.9	18
Nanosized Cu	2.5	2.75	230	2	77.5	59.3	19
$CuAu_2$	3.0	3.3	200	2	95.8	87.1	This work
$CuAu_3$	3.0	3.3	200	2	96.0	84.9	This work
$CuAu_4$	3.0	3.3	200	2	97.4	83.5	This work

yields of lactic acid of 92.7%, 89.7%, and 87.2% were obtained at the catalyst loading of 0.736 g. The highest yield of lactic acid was obtained over the bimetallic $CuAu_2$ catalyst while the carbon balance was of the highest value of 95.4%. The selectivities of by-products were less than 1.6% even though the catalyst loading was 0.920 g.

The catalytic activities for glycerol conversion over the bimetallic $CuAu_x$ catalysts increased with the increase in Au contents. The presence of Au in the bimetallic $CuAu_x$ catalyst enhanced its catalytic activity.

The typical results of the present work and the previously reported results are summarized in Table 5. The presence of $CuAu_x$ catalysts decreased the reaction temperature by 80 °C as compared to the hydrothermal method.[11,12] The $CuAu_x$ catalysts gave higher lactic acid yield at a higher glycerol concentration than the noble metal catalysts.[14,16] The bimetallic $CuAu_x$ catalysts favored the catalytic conversion of glycerol to lactic acid as compared to the supported and nanosized metallic copper catalysts.[17–19] The interaction between Au and Cu played an important role for the formation of lactic acid from glycerol.

3.5. Recycling performance of bimetallic $CuAu_2$ nanoparticle catalyst

Considering the prominent performance of the bimetallic $CuAu_2$ catalyst, it was selected as the model catalyst to investigate its stability and recycling performance. The results are shown in Fig. 7. After reacting at 200 °C for 2 h, the used catalyst was separated from reaction solution by centrifugation at 8000 rpm and dried at 60 °C in a vacuum oven for 4 h before next recycling. For the fresh $CuAu_2$ nanoparticle catalyst, the glycerol conversion and lactic acid selectivity were 99.0% and 93.8%, respectively. And after recycling for six times, the glycerol conversion and lactic acid selectivity were 95.0% and 91.9%, respectively. According to the recycling experimental results, it was found that the $CuAu_2$ catalyst exhibited good recycling performance.

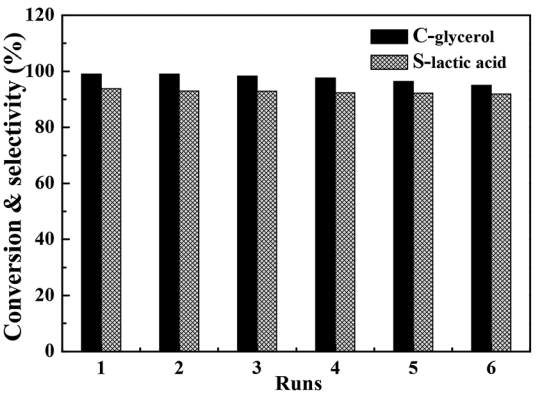

Fig. 7 Recycling performance of the bimetallic $CuAu_2$ nanoparticle catalyst. Reaction conditions for each run: 100 mL of glycerol aqueous solution with the glycerol concentration of 2 mol L^{-1}; NaOH/glycerol mole ratio of 1.1 : 1; 0.736 g of catalyst; reaction temperature, 200 °C; reaction time, 2 h.

After recycling for six times, the Cu/Au atomic ratios in the spent $CuAu_2$ catalyst was 100 : 1.93, indicating that the bimetallic $CuAu_2$ catalyst was stable during the catalytic reaction.

3.6. Reaction kinetics

3.6.1. Preliminary consideration. A power-function type reaction kinetic equation (eqn (2)) was used to investigate the effect of glycerol and NaOH concentrations and reaction temperature on the catalytically hydrothermal conversion of glycerol over the bimetallic $CuAu_x$ catalysts. The reaction order and activation energy were fitted according to the data at lower reaction temperatures of 110–140 °C. Considering that glycerol could not be completely converted to desired lactic acid at a lower reaction temperature. The reaction kinetics aimed at the correlation among the consumption rate of glycerol, the concentrations of glycerol and NaOH, and reaction temperature.

In order to eliminate the effect of diffusion, the bimetallic $CuAu_x$ catalysts with different loadings in a range of 0.092–0.328 g were used for the catalytic conversion of glycerol at 140 °C and a stirring speed of 600 rpm with the initial glycerol and NaOH concentrations of 1.0 and 1.1 mol L^{-1}, respectively. A linear correlation between the catalyst loading and the glycerol conversion was obtained (Fig. S4†), which indicating the reaction was controlled by chemical reaction rather than mass diffusion.[23,24]

Raising the autoclave temperature to the prescribed reaction temperature needed *ca.* 0.5 h without stirring. And glycerol was almost not converted during the time period for raising reaction temperature. Moreover, when the reaction was carried out over the bimetallic $CuAu_x$ catalysts under stirring at 600 rpm or 1000 rpm for 1 h, the glycerol conversions were close to each other, indicating that the diffusion effect was eliminated under stirring at 600 rpm.

The power-function type reaction kinetic equation is expressed as follows.

$$-r_A = -dn_A/(m_{cat}dt) = kC_A{}^aC_B{}^b \quad (2)$$

where $-r_A$ is the glycerol consumption rate, mol $g_{cat}{}^{-1}$ h^{-1}; m_{cat} is the amount of catalyst, g; n_A is the mole number of glycerol, mol; t is the reaction time, h; C_A and C_B are the glycerol and NaOH concentrations, mol L^{-1}; a and b are the reaction orders with respect to the concentrations of glycerol and NaOH, respectively.

The rate constant k follows the Arrhenius equation.

$$k = A\exp(-E_a/(RT)) \quad (3)$$

where k is the rate constant; A is the pre-exponential (frequency) factor; R is the ideal gas constant, 8.314×10^{-3} kJ mol^{-1} K^{-1}; E_a is the reaction activation energy, kJ mol^{-1}; and T is the reaction temperature, K.

3.6.2. Reaction order. Eqn (4) was obtained by taking the natural logarithm of both sides of the eqn (2), as follows.

$$\ln(-r_A) = \ln k + a\ln C_A + b\ln C_B \quad (4)$$

To calculate the reaction orders of a and b according to eqn (4), the initial conversion rates of glycerol were calculated according to the data shown in Table 6, which shows the glycerol conversions at 140 °C under different initial concentrations of glycerol and NaOH. The initial conversion rates of glycerol at 140 °C under different initial concentrations of glycerol and NaOH were calculated at the first hour.

Fig. 8a shows the lines by plotting $\ln(-r_A)$ *vs.* $\ln C_A$ over the bimetallic $CuAu_x$ nanoparticle catalysts. The data used in Fig. 8a were calculated according to those shown in Table 6, straight lines were obtained while plotting $\ln(-r_A)$ *vs.* $\ln C_A$. The straight lines over the $CuAu_1$, $CuAu_2$, $CuAu_3$, and $CuAu_4$ catalysts gave good linear correlations of 0.9826, 0.9892, 0.9863 and 0.9793, respectively. The reaction orders of glycerol over the $CuAu_1$, $CuAu_2$, $CuAu_3$, and $CuAu_4$ nanoparticle catalysts are 0.56, 0.62, 0.49, and 0.56, respectively (Table 7).

Fig. 8b shows the lines by plotting $\ln(-r_A)$ *vs.* $\ln C_B$ over the bimetallic $CuAu_x$ nanoparticle catalysts. The data used in Fig. 8b were calculated according to those shown in Table 6, straight lines were obtained while plotting $\ln(-r_A)$ *vs.* $\ln C_B$. The

Table 6 Glycerol conversions under different reaction conditions over the $CuAu_x$ nanoparticle catalysts for reaction kinetics simulation[a]

Reaction conditions			Glycerol conversions (%)			
Glycerol concentrations (mol L^{-1})	NaOH/glycerol molar ratios	Reaction temperatures (°C)	$CuAu_1$	$CuAu_2$	$CuAu_3$	$CuAu_4$
0.5	1.1	140	18.6	22.7	27.2	34.6
1.0	1.1	140	15.4	19.3	21.6	29.7
1.5	1.1	140	13.4	15.5	18.6	22.7
2.0	1.1	140	10.5	12.4	14.4	17.6
1.0	0.5	140	7.8	13.6	15.4	20.1
1.0	1.0	140	9.2	16.7	17.4	26.1
1.0	1.1	140	15.4	19.3	21.6	29.7
1.0	1.5	140	18.6	23.2	27.2	33.1
1.0	1.1	110	3.6	6.8	7.5	12
1.0	1.1	120	5.6	8.8	11.9	17.2
1.0	1.1	130	11.2	15.4	17.3	21.6
1.0	1.1	140	15.4	19.3	21.6	29.7

[a] Reaction conditions: glycerol aqueous solution, 100 mL; catalyst, 0.276 g; reaction time, 1.0 h.

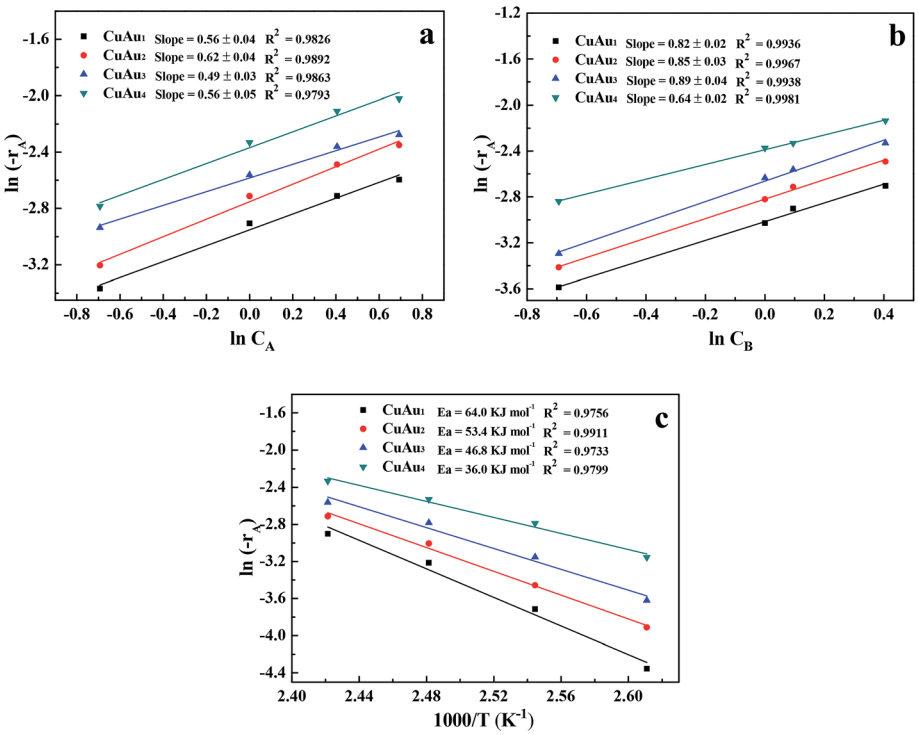

Fig. 8 Estimation of (a and b) the reaction orders and (c) the reaction activation energies for the power-function type reaction kinetics over the bimetallic $CuAu_x$ nanoparticle catalysts.

Table 7 Initial reaction rates and reaction orders of glycerol and NaOH over the bimetallic $CuAu_x$ nanoparticle catalysts[a]

	Initial concentrations of glycerol and NaOH (mol L^{-1})									
	0.5, 1.1	1.0, 1.1								
Catalysts	$-rA$ (mol g_{cat}^{-1} h^{-1})		1.5, 1.1	2.0, 1.1	1.0, 0.5	1.0, 1.0	1.0, 1.5	a	R^2	b	R^2
$CuAu_1$	0.0344	0.0549	0.0664	0.0746	0.0277	0.0484	0.0670	0.56 ± 0.04	0.9826	0.82 ± 0.02	0.9936
$CuAu_2$	0.0405	0.0664	0.0830	0.0954	0.0329	0.0595	0.0827	0.62 ± 0.04	0.9892	0.85 ± 0.03	0.9967
$CuAu_3$	0.0530	0.0771	0.0943	0.1025	0.0371	0.0718	0.0973	0.49 ± 0.03	0.9863	0.89 ± 0.04	0.9938
$CuAu_4$	0.0618	0.0971	0.1214	0.1325	0.0585	0.0932	0.1182	0.56 ± 0.05	0.9793	0.64 ± 0.02	0.9981

[a] a and b are the reaction orders for glycerol and NaOH, respectively.

straight lines over the $CuAu_1$, $CuAu_2$, $CuAu_3$, and $CuAu_4$ catalysts gave good linear correlations of more than 0.9936, respectively. The reaction orders of NaOH over the $CuAu_1$, $CuAu_2$, $CuAu_3$, and $CuAu_4$ nanoparticle catalysts are 0.82, 0.85, 0.89, and 0.64, respectively (Table 7).

The power-function type reaction kinetic eqn (5)–(8) over the $CuAu_1$, $CuAu_2$, $CuAu_3$, and $CuAu_4$ nanoparticle catalysts can be written as follows.

$$-r_A = -dn_A/(m_s dt) = kC_A^{0.56}C_B^{0.82} \quad (5)$$

$$-r_A = -dn_A/(m_s dt) = kC_A^{0.62}C_B^{0.85} \quad (6)$$

$$-r_A = -dn_A/(m_s dt) = kC_A^{0.49}C_B^{0.89} \quad (7)$$

$$-r_A = -dn_A/(m_s dt) = kC_A^{0.56}C_B^{0.64} \quad (8)$$

3.6.3. Activation energy. Combining eqn. (3) and (5)–(8), the reaction kinetic equations over the $CuAu_1$, $CuAu_2$, $CuAu_3$, and $CuAu_4$ nanoparticle catalysts can be rearranged as follows.

$$-r_A = A\exp(-E_a/(RT))C_A^{0.56}C_B^{0.82} \quad (9)$$

$$-r_A = A\exp(-E_a/(RT))C_A^{0.62}C_B^{0.85} \quad (10)$$

$$-r_A = A\exp(-E_a/(RT))C_A^{0.49}C_B^{0.89} \quad (11)$$

$$-r_A = A\exp(-E_a/(\mathrm{RT}))C_A^{0.56}C_B^{0.64} \quad (12)$$

By taking the natural logarithm of both sides of eqn (9)–(12), the equations can be rearranged as follows.

$$\ln(-r_A) = \ln(AC_A^{0.56}C_B^{0.82}) - E_a/(RT) \quad (13)$$

$$\ln(-r_A) = \ln(AC_A^{0.62}C_B^{0.85}) - E_a/(RT) \quad (14)$$

$$\ln(-r_A) = \ln(AC_A^{0.49}C_B^{0.89}) - E_a/(RT) \quad (15)$$

$$\ln(-r_A) = \ln(AC_A^{0.56}C_B^{0.64}) - E_a/(RT) \quad (16)$$

The data listed in the Table 6 were used to calculate the initial reaction rates, $-r_A$, at different reaction temperatures of 110–140 °C over the $CuAu_1$, $CuAu_2$, $CuAu_3$, and $CuAu_4$ nanoparticle catalysts, respectively. According to the eqn (13)–(16), four straight lines with good linear correlations of more than 0.9733, respectively, were obtained while plotting $\ln(-r_A)$ *vs.* $1/T$ (Fig. 8c). From the slopes and intercepts of the straight lines, the activation energies (E_a) and frequency factors (A) were obtained, which are listed in Table 8. Over the $CuAu_1$, $CuAu_2$, $CuAu_3$, and $CuAu_4$ nanoparticle catalysts, the reaction kinetic equations are listed as follows, respectively.

$$-r_A = -dn_A/(m_{cat}dt) = 7.50 \times 10^6 \exp(-64.0/(RT))C_A^{0.56}C_B^{0.82} \quad (17)$$

$$-r_A = -dn_A/(m_{cat}dt) = 3.88 \times 10^5 \exp(-53.4/(RT))C_A^{0.62}C_B^{0.85} \quad (18)$$

$$-r_A = -dn_A/(m_{cat}dt) = 6.75 \times 10^4 \exp(-46.8/(RT))C_A^{0.49}C_B^{0.89} \quad (19)$$

$$-r_A = -dn_A/(m_{cat}dt) = 3.57 \times 10^3 \exp(-36.9/(RT))C_A^{0.56}C_B^{0.64} \quad (20)$$

The activation energies for the bimetallic $CuAu_1$, $CuAu_2$, $CuAu_3$, and $CuAu_4$ nanoparticle catalysts were 64.0, 53.4, 46.8,

Table 8 Initial reaction rates, frequency factors, and reaction activation energies over bimetallic $CuAu_x$ nanoparticle catalysts[a]

	$-rA$ (mol g^{-1} h^{-1})						
Catalysts	110 °C	120 °C	130 °C	140 °C	A ($mol^{1-(a+b)}$ $g_{cat}^{(a+b)-1}$ h^{-1})	E_a (kJ mol^{-1})	R^2
$CuAu_1$	0.0129	0.0244	0.0401	0.0549	7.50×10^6	64.0	0.9756
$CuAu_2$	0.0200	0.0315	0.0496	0.0664	3.88×10^5	53.4	0.9911
$CuAu_3$	0.0268	0.0430	0.0619	0.0771	6.75×10^4	46.8	0.9733
$CuAu_4$	0.0426	0.0615	0.0797	0.0971	3.57×10^3	36.9	0.9799

[a] A is the frequency factor, and E_a is the reaction activation energy.

and 36.9 kJ mol^{-1}, respectively. The activation energies and frequency factors decreased with increasing the Au content in the bimetallic $CuAu_x$ nanoparticle catalysts. The results indicated that the Au contents in the bimetallic catalysts affected their activation energies and reaction orders.

3.7. Reaction routes

Based on the analysis in the paragraph 3.4.1, the co-presence of the bimetallic $CuAu_x$ catalyst and NaOH effectively catalyzed the conversion of high-concentrated glycerol to lactic acid. According to the findings in our present work and the reported reaction pathways for the catalytically hydrothermal conversion of glycerol to lactic acid in an aqueous solution,[11,12,25] the reaction routes over the bimetallic $CuAu_x$ nanoparticle catalysts in an alkaline solution are discussed as follows.

It was speculated that the catalytic dehydrogenation of glycerol to glyceraldehyde was the first step,[13,26] which was a crucial step for the whole reaction. The bimetallic $CuAu_x$ nanoparticle catalysts play an important role in the catalytic dehydrogenation of terminal hydroxyl group of glycerol to glyceraldehyde. Then in a basic environment, the 2-hydroxypropenal was formed *via* the intramolecular dehydration of glyceraldehyde.[18,25] Pyruvaldehyde was conveniently formed from 2-hydroxypropenal *via* the keto–enol tautomerization.[26] The resultant pyruvaldehyde was converted to lactate *via* the Cannizzaro reaction.[12,15,16,18]

In addition, the by-products, such as 1,2-propanediol, formic acid, acetic acid, oxalic acid, existed in our present experiments, which probably formed in the following routes. There were three routes for the formation of 1,2-propanediol, the catalytic hydrogenation of glycerol with resultant H_2 could produce 1,2-propanediol, and both 2-hydroxypropenal and pyruvaldehyde could also be hydrogenated to 1,2-propanediol over the bimetallic $CuAu_x$ nanoparticle catalysts. The acetate and formate anions were formed by the decomposition of lactate anions in an alkaline solution, accompanied with the formation of carbonate anions.[9] Oxalate anions were probably from the oxidative cleavage of glyceraldehyde in an alkaline solution.[27]

Some intermediates, such as pyruvaldehyde, glyceraldehyde, and 2-hydroxypropenal, were not detected under our present experimental conditions at the reaction temperature of above 200 °C, indicating that these intermediates could be rapidly converted to subsequent chemicals and finally to lactate.

4. Conclusions

The bimetallic $CuAu_x$ nanoparticles were prepared by the wetness chemical reduction method successfully. Metallic Cu and Au nanoparticles with the average particle sizes of *ca*. 13 and 5 nm were formed in the bimetallic $CuAu_x$ nanoparticles. Based on the XRD and XPS analyses, there existed an alloy trend between Cu and Au nanoparticles.

The bimetallic $CuAu_x$ nanoparticles effectively catalyzed the hydrothermal conversion of high-concentrated glycerol to lactic acid at a relative low reaction temperature of 200 °C. The catalytic activities of the bimetallic $CuAu_x$ nanoparticles were higher than those of the monometallic Cu and Au nanoparticles. When the catalytic hydrothermal conversion of glycerol (2 mol L^{-1}) over the bimetallic $CuAu_2$ nanoparticles in an alkaline solution was carried out at 200 °C for 2 h, the selectivity of lactic acid was 93.8% at the conversion of glycerol of 99.0%. The $CuAu_2$ nanoparticle catalyst exhibited good recycling performance and stability. Over the bimetallic $CuAu_1$, $CuAu_2$, $CuAu_3$, and $CuAu_4$ nanoparticle catalysts, the power-function type reaction kinetic model well fitted the experimental data, and the reaction activation energies were 64.0, 53.4, 46.8, and 36.9 kJ mol^{-1}, respectively.

Acknowledgements

The work was financially supported by the funds from National Natural Science Foundation of China (21506078 and 21506082), China Postdoctoral Science Foundation (2016M601739) and Science and Technology Department of Jiangsu Province of China (BY2014123-10).

References

1 Z. Lu, I. Demianets, R. Hamze, N. J. Terrile and T. J. Williams, *ACS Catal.*, 2016, **6**, 2014–2017.
2 M. R. A. Arcanjo, I. J. S. Júnior, E. Rríguez-Castellón, A. Infantes-Molina and R. S. Vieira, *Catal. Today*, 2017, **279**, 317–326.
3 S. Adhikari, S. D. Fernando and A. Haryanto, *Renew. Energ.*, 2008, **33**, 1097–1100.
4 Global Glycerol Market Size, Market Share, Application Analysis, Regional Outlook, Growth, Trends, Competitive Scenario and Forecasts, 2012 to 2020, http://www.hexaresearch.com/research-report/glycerol-industry.
5 European Commission, The impact of biofuels on transport and the environment, and their connection with agricultural development in Europe, *Directorate General for the Internal Policies Policy Department B: Structural and Cohesion Policies-Transport and Tourism*, Brussells, 2015, http://www.europarl.europa.eu/RegData/etudes/STUD/2015/513991/IPOL_STU(2015)513991_EN.pdf.
6 D. Gambelli, F. Alberti, F. Solfanelli, D. Vairo and R. Zanoli, *Energy Policy*, 2017, **103**, 165–178.
7 L. E. Hombach, C. Cambero, T. Sowlati and G. Walther, *J. Cleaner Prod.*, 2016, **133**, 565–575.
8 C. Zhang, T. Wang, X. Liu and Y. J. Ding, *Chin. J. Catal.*, 2016, **37**, 502–509.
9 U.S. Department of Agriculture, *Final Report: Renewable Chemicals & Materials Opportunity Assessment*, 2014, http://www.usda.gov/oce/reports/energy/USDA_RenewChems_Jan2014.pdf.
10 M. A. Abdel-Rahman, Y. Tashiro and K. Sonomoto, *Biotechnol. Adv.*, 2013, **31**, 877–902.
11 H. Kishida, F. Jin, Z. Zhou, T. Mory and H. Enomoto, *Chem. Lett.*, 2005, **34**, 1560–1561.
12 C. A. Ramírez-López, J. R. Ochoa-Gómez, M. Fernández-Santos, O. Goméz-Jiménez-Aberasturi, A. Alonso-Vicario

and J. Torrecilla-Soria, *Ind. Eng. Chem. Res.*, 2010, **49**, 6270–6278.
13 J. Ftouni, N. Villandier, F. Auneau, M. Besson, L. Djakovitch and C. Pinel, *Catal. Today*, 2015, **257**, 267–273.
14 Y. H. Shen, S. H. Zhang, H. J. Li, Y. Ren and H. C. Liu, *Chem.–Eur. J.*, 2010, **16**, 7368–7371.
15 P. Lakshmanan, P. P. Upare, N. T. Le, Y. K. Hwang, D. W. Hwang, U. H. Lee, H. R. Kim and J. S. Chang, *Appl. Catal., A*, 2013, **468**, 260–268.
16 R. K. P. Purushothaman, J. V. Haveren, D. S. V. Es, I. Melián-Cabrera, J. D. Meeldijk and H. J. Heeres, *Appl. Catal., B*, 2014, **147**, 92–100.
17 D. Roy, B. Subramaniam and R. V. Chaudhari, *ACS Catal.*, 2011, **1**, 548–551.
18 H. Yin, C. Zhang, H. Yin, D. Gao, L. Shen and A. Wang, *Chem. Eng. J.*, 2016, **288**, 332–343.
19 H. Yin, H. Yin, A. Wang, L. Shen, Y. Liu and Y. Zheng, *J. Nanosci. Nanotechnol.*, 2017, **17**, 1255–1266.
20 H. Yin, Y. Wada, T. Kitamura, S. Kambe, S. Murasawa, H. Mori, T. Sakata and S. Yanagida, *J. Mater. Chem.*, 2001, **11**, 1694–1703.
21 S. Poulston, P. M. Parlett, P. Stone and M. Bowker, *Surf. Interface Anal.*, 1996, **24**, 811–820.
22 D. Zhang, H. Yin, J. Xue, C. Ge, T. Jiang, L. Yu and Y. Shen, *Ind. Eng. Chem. Res.*, 2009, **48**, 11220–11224.
23 Y. H. Feng, H. B. Yin, D. Z. Gao, A. L. Wang, L. Q. Shen and M. J. Meng, *J. Catal.*, 2014, **316**, 67–77.
24 X. Huang, X. Wang, X. Wang, X. Wang, M. Tan, W. Ding and X. Lu, *J. Catal.*, 2013, **301**, 217–226.
25 L. Chen, S. J. Ren and X. P. Ye, *Fuel Process. Technol.*, 2014, **120**, 40–47.
26 F. Auneau, C. Michel, F. Delbecq, C. Pinel and P. Sautet, *Chem.–Eur. J.*, 2011, **17**, 14288–14293.
27 F. Auneau, L. S. Arani, M. Besson, L. Djakovitch, C. Michel, F. Delbecq, P. Sautet and C. Pinel, *Top. Catal.*, 2012, **55**, 474–479.